Appl Phys A (2011) 102: 13–19
DOI 10.1007/s00339-010-6040-2

Applied Physics A
Materials Science & Processing

INVITED PAPER

Nanoscale amorphization, bending and recrystallization in silicon nanowires

Emanuele F. Pecora · Alessia Irrera · Simona Boninelli · Lucia Romano · Corrado Spinella · Francesco Priolo

Received: 26 August 2010 / Accepted: 30 August 2010 / Published online: 8 September 2010

Abstract Controllable and uniform doping of nanowires (NWs) is the ultimate challenge prior to their effective application. Si NWs amorphize and bend toward the impinging ions under ion irradiation as a result of viscous flow. We demonstrate that thermal annealing induces a full recovery of the crystalline phase corresponding to the unbending of the NWs. The competition between Solid Phase Epitaxy and Random Nucleation and Growth at the nanoscale is the key parameter controlling the recovery.

1 Introduction

In very recent years much attention has been reserved to semiconductor nanowires (NWs) as building blocks for a wide range of future nanoscale devices. They exhibit novel electronic [1, 2] and optical (both as emitter and photovoltaic elements) properties [3, 4] and they are candidates as organic and inorganic sensors [5] and anodes of high-performance batteries [6]. Their unique structure exhibits carrier quantum confinement in the planar directions and a high surface/volume ratio. They can be prepared following a bottom-up approach leading to a precise tailoring of their structural properties as well as crystallographic properties. Effective NW doping represents the ultimate challenge for the transition from research prototype to large scale devices. The possibility to insert and activate both n- and p-type dopants has been explored since the early works on NW growth. Many attempts have been explored referring both to in- and ex-situ methods, but the major drawbacks are still the segregation of the dopants at the surface and the non-uniform doping along the NW length [7–9]. Ion implantation represents the effective and hopeful pathway to obtain uniform doping for constant electrical properties [10], and it could allow a direct integration of the NW in the current CMOS technology. In very recent years some works have reported the investigation of the electrical properties of implanted nanowires [11, 12], but the ion-irradiation effects and the crystallographic damage, which could limit the electrical performance of the implanted dopant ions, are still mostly unexplored. Recently, bending of GaAs NWs using ion beam irradiation has been observed, and the spatial separation between interstitials and vacancies within the ion tracks has been proposed as the key mechanism for bending [13]. Moreover, focused ion beam-assisted nanoscale manipulation of Ge [14], Si [15] NWs and C-nanotubes [16] has been reported. However, while the deformation under ion irradiation of Si NWs has been observed, the bending mechanism itself has not fully understood and, more importantly, the possibility to recover the structural modifications occurring in consequence of the irradiation has never been investigated. In addition, amorphization of single Si NWs has been observed during electron transport measurements before and after lithiation [6], thus it is important to explore the possibility to drive back to the origin. Although still unexploited, annealing procedures are required in order

E.F. Pecora · A. Irrera (✉) · S. Boninelli · L. Romano · F. Priolo
MATIS IMM-CNR, Via S. Sofia, 64, 95123 Catania, Italy
e-mail: alessia.irrera@ct.infn.it
Fax: +39-095-3785243

E.F. Pecora · L. Romano · F. Priolo
Department of Physics and Astronomy, University of Catania, Via S. Sofia, 64, 95123 Catania, Italy

C. Spinella
CNR-IMM, VIII Strada, 5, 95125 Catania, Italy

E.F. Pecora
CSFNSM, Viale A. Doria, 6, 95125 Catania, Italy

to activate the dopants [17], but their effects on the structure of the NWs are unknown. These processes have been studied in bulk structures, the only examples at the nanoscale are nanocrystals embedded into a matrix, while NWs can be considered quasi-free standing system. We investigate the Si NWs structural and crystallographic evolution during ion implantation and thermal annealing. Inclined Si NWs bend under ion irradiation and the bending is reversible after subsequent thermal annealing. The results are interpreted and elucidate the damage mechanisms and the recovery kinetics, opening the way for a precise control of the NW doping and a direct integration of the NW synthesis in the microelectronic mainstream.

2 Experimental

Epitaxial Si NWs were grown on (111)-oriented Si substrates through electron beam evaporation [18, 19]. (111)-oriented Si wafers were first UV oxidized and dipped in HF in order to clean the surface. They were then immediately loaded within the vacuum chamber. Both Au and Si sources were stored inside the same deposition chamber having a base pressure of 1–2 $\times$ 10^{-8} mbar. Sources were evaporated using a focused electron beam with a maximum power of 3 kW. The evaporation flux was monitored in-situ by a calibrated quartz microbalance (Inficon); the distance between the source and the sample ($\sim$30 cm) ensured a homogeneous deposition over a 2 $\times$ 2 cm^2 area. During deposition, the flux has been maintained constant at 2.5 $\times$ 10^{14} cm^{-2} s^{-1} at the position of the substrate. The sample was eventually heated through the Joule effect. A 2 nm-thick Au layer was firstly evaporated maintaining the sample at room temperature. After deposition, the sample was annealed at 700°C for 2 hours in order to induce the continuous Au layer breaking and the formation of Au droplets on the substrate. After cluster preparation, the temperature was reduced to 510°C for the Si evaporation and NWs growth. The Si fluence was fixed at 2.5 $\times$ 10^{18} cm^{-2}. Si NWs were implanted with 45 keV Ge ions extracted from an HVEE ion implanter. Ge ions impinge with a direction perpendicular to the substrate. The 45 keV beam energy, corresponding to a projected range of about 30 nm,[1] has been chosen in such a way that the implanted ion profile is fully inside the NW. Ge fluences were varied from 1 $\times$ 10^{13} up to 2.5 $\times$ 10^{15} cm^{-2}. The recovery of the damage has been investigated by thermal annealing in a furnace under nitrogen flux. Structural characterization was performed by a field emission scanning electron microscope (FE-SEM) Zeiss Supra 25 and by a 200 kV transmission electron microscope Jeol JEM 2010F. A Gatan Digital Microscope software was used for the statistical analyses.

[1] http://www.srim.org.

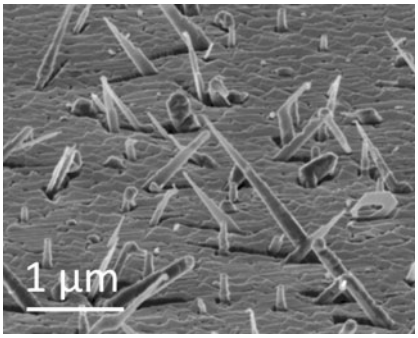

Fig. 1 SEM image of the as-deposited sample prepared evaporating a Si fluence of 2.5 $\times$ 10^{18} cm^{-2} at a substrate temperature of 510°C

3 Results and discussion

Figure 1 reports a Scanning Electron Microscopy (SEM) image of the as-deposited sample containing Si NWs. NWs belonging to three different crystallographic orientations have been identified [18, 19]. (111)-oriented NWs are perpendicular to the substrate and they have a mean length of $\sim$300 nm, (110)-oriented NWs form an angle of 45° and (100)-oriented NWs an angle of 54°. Both the latter inclined NWs families are tapered and their length is of about 900 nm with a mean radius measured at the basis equal to 49 $\pm$ 16 nm.

The NWs have been then implanted with a 45 keV Ge ion beam perpendicular to the substrate in such a way that the ions impinge on the NWs surface forming an angle of about 45°. After Ge implantation with fluences below 5 $\times$ 10^{14} cm^{-2} we do not observe any modification in the structure of the NWs. On the other hand, the effects of the ion beam are very impressive in the inclined NWs of the sample implanted with fluences higher than 5 $\times$ 10^{14} cm^{-2}. As an example, the SEM image reported in Fig. 2(a) is a high magnification of a NW representative of the population of the inclined NWs after implantation with fluence of 1 $\times$ 10^{15} cm^{-2}. It is straightforward to note that the top of the NW structure is modified in such a way that it bends toward the beam while the bottom part of the NW remains unaffected.

In order to gain more quantitative information, we analyzed the structural features of hundreds of bent NWs in order to get a significant statistical analysis. Figure 2(b) reports the histogram graph of the absolute density of bent NWs as a function of the measured bending angle θ_{bend} formed between the substrate and the direction of the bent portion of the NW in the samples implanted with fluences of 5 $\times$ 10^{14} and 1 $\times$ 10^{15} cm^{-2}. This angle is related to the NW curvature, but it directly represents how the direction of the NW has been modified in consequence of the irradiation. Note that the initial (in the as-deposited sample) angle formed between the NW and the substrate is 45°

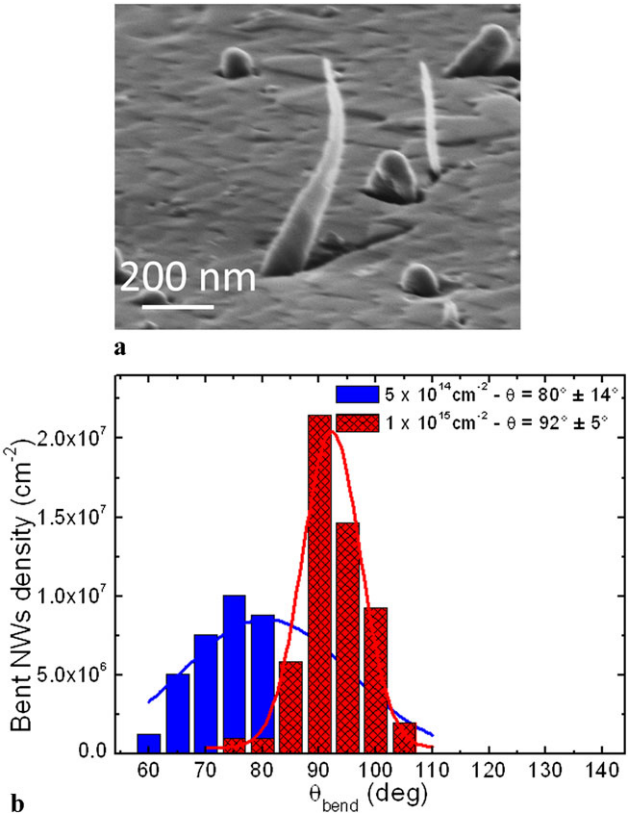

Fig. 2 (**a**) High-magnification SEM image of an inclined NW, which has bent after irradiation with Ge ions of 45 keV up to fluence of 1×10^{15} cm^{-2}. (**b**) Histogram graph of the absolute density of bent NWs as a function of the measured angle θ_{bend} in the samples implanted with the fluences of 5×10^{14} and 1×10^{15} cm^{-2}

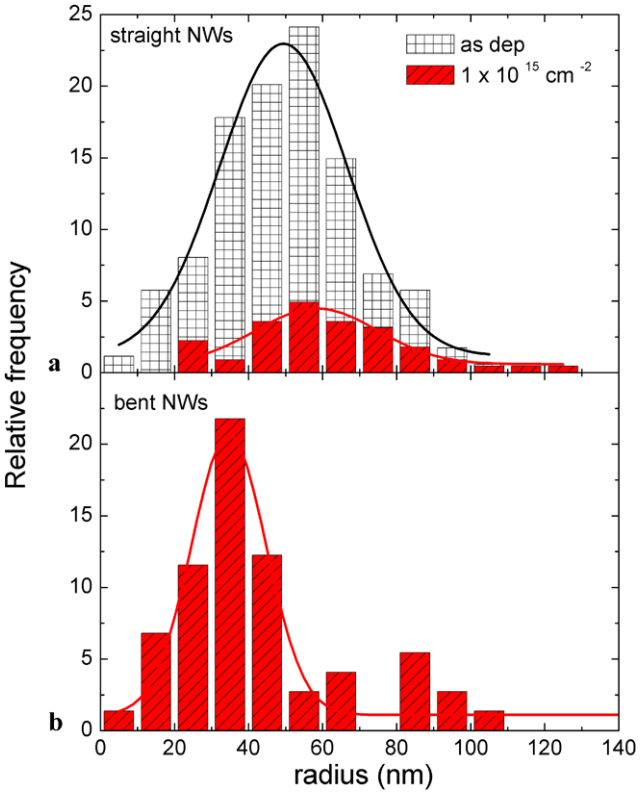

Fig. 3 Histogram plots of the relative density of straight (**a**) and bent (**b**) NWs as a function of their radius after the implantation up to fluence of 1×10^{15} cm^{-2}. As a reference, the radius distribution in the as-deposited sample is reported in the panel (**a**). Continuous lines are the fits of the histograms according to a Gaussian function

or 54°, depending on the crystallographic orientation. The continuous lines represent a Gaussian fit of the data. The best-fit values are reported inside the graph. For a fluence of 5×10^{14} cm^{-2} (blue bars), we measured a wide range of possible θ_{bend}, from 60° to 85°. This fluence is the threshold for NWs bending and the increasing angle (with respect to the original ones) demonstrates that NWs start to move upward since the beginning of the deformation process. Afterward, for all the higher implantation fluences the distribution is always centered at around 90°, as shown as an example by the red columns referring to a fluence of 1×10^{15} cm^{-2}. Note that the FWHM of this fit is equal to the standard error of the measurements. The bent portion of the NW has been deformed in order to align itself toward the direction of the ion beam (with the tip of the NWs pointing to the incoming ions). These data demonstrate that ion-irradiated Si NWs modify their structure in such a way as to minimize the exposed surface to the beam. By further increasing the implanted fluence in a wide range up to 2.5×10^{15} cm^{-2}, the structural features of the NWs do not change anymore, contrary to what has already been observed in literature in the case of NWs of different semiconductors [13–15].

A complete analysis of the NW bending is offered by the investigation of the size effects on the structural modifications of the NWs. Figure 3 reports the histogram plots of the relative density of straight (a) and bent (b) NWs as a function of their radius after the implantation at a fluence of 1×10^{15} cm^{-2}. As a reference, the radius distribution in the as-deposited sample is also reported. Continuous lines are fits of the histograms according to a Gaussian function. The as-deposited sample shows a wide radius distribution. After irradiation, about 70% of the NWs have bent and the mean radius of the relative distribution is of 34 ± 10 nm. The straight NWs, which have not been affected by the ion implantation process, are reported in panel (a); they are the biggest ones, exhibiting a mean radius of 58 ± 16 nm. Therefore, the bending effect is evident only in the NWs with the smallest size, while the biggest ones remaining unaffected.

In order to correlate the bending effects to the microscopic structure of the NWs we performed a detailed crystallographic analysis on several NWs through Transmission Electron Microscopy (TEM). Figure 4(a) shows a bright field image of a portion of an irradiated NW. The bottom part corresponds to the unaffected region, and the bending of the upper part is clearly visible. From selected areas of the

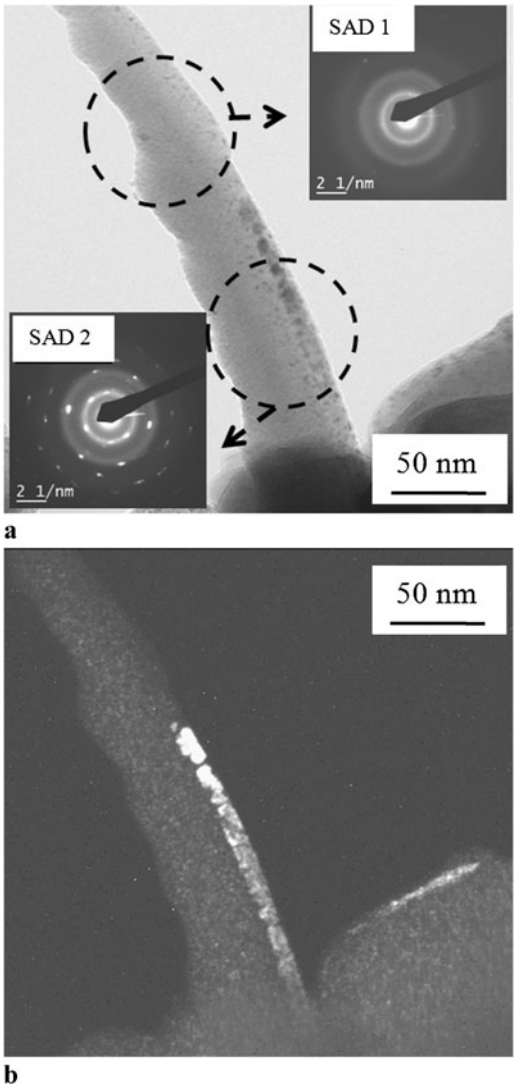

Fig. 4 (**a**) Bright field TEM image of a portion of an irradiated NW. In the insets, the SAD patterns of the bent and of the unaffected region are showed. (**b**) Dark field TEM image of the same NW obtained selecting the (111) diffraction spot

image the corresponding selected area diffraction patterns (SAD) were obtained. In the insets, the SAD patterns of the bent and of the unaffected region are shown respectively. The first one (SAD1) indicates that the bent region is fully amorphous; on the contrary from the second pattern (SAD2) we deduce that the amorphous and crystalline structures coexist. The dark field image obtained selecting the (111) diffraction spot is also shown in Fig. 4(b). It reveals the presence of a crystal/amorphous interface inside the NW itself as a consequence of the ion irradiation. These data are consistent with a simulation of the ion beam irradiation using the TRIM code (see footnote 1). In fact, we can deduce that in the inclined NWs a 45 keV Ge beam has a projected range of ∼30 nm. Hence while in the top tapered portion of the NW the beam is passing through (and can amorphize it completely), in then bottom region only part of the NW can be amorphized and part will remain unaffected. In addition, it is calculated that the Ge dose to produce 0.3 displacements per atom (which is the threshold for amorphization of bulk Si [20]) is 5×10^{14} cm^{-2}. This observation suggests that bending is related to the amorphization process and starts as soon as amorphization takes place. In the past years, the effects of high-energy irradiation on amorphous microstructures have been investigated [21–23]. A viscoelastic spike model [24] has been proposed to explain the observed anisotropic plastic deformation at constant volume. The ion beam penetrating the material induces an anisotropic heating of a cylindrical region around the ion track depending on the electronic energy losses during the collisional cascade. The thermal expansion brings shear stress that then relaxes, resulting in a local in-plane expansion. The net effect consists in an expansion in the direction perpendicular to the ion track and a shrinking in the direction parallel to the ion beam, in order to maintain the volume constant. This effect requires the material to be amorphous because of the presence of shear sites (regions with a local free volume) and it has not been observed in crystalline materials. While these effects have typically been observed at very high ion beam energies (at which the electronic energy loss is higher), one might expect at the nanoscale that it is possible also at lower energies. Indeed, we propose that the top tapered part of the Si NWs, which is fully amorphized, experiences this deformation, which induces the observed bending.

Another question arises on the role (if any) of the crystal/amorphous interface. To answer this question we have irradiated a sample with a 300 keV Ge beam at a dose of 1×10^{15} cm^{-2}. The energy is such that the beam is passing through for the entire length of the NW and the dose is well above the amorphization threshold. In this irradiation Si NWs are fully amorphized (as also verified by TEM) but no bending effect is observed. These results demonstrate that the presence of a crystal/amorphous interface is playing a crucial role in the bending process. In fact the crystalline strip represents a strong structural constrain forcing this NW portion to remain straight. On the contrary, the totally amorphous region bends because of the plastic deformation due to the irradiation. Furthermore, it should be noted that the bending effect is evident only in the NWs which were not perpendicular to the substrate, i.e. parallel to the ion beam. In fact the (111)-oriented NWs remain always straight (as confirmed by SEM images not shown); in this case the ion beam penetrates no more than ∼60 nm from the top, thus forming an axial structure in which the very top part is totally amorphous, while the other remains crystalline. This structure is stable and it does not need for a bending to accommodate the structural stress.

If deformation is indeed associated with the presence of a crystal/amorphous interface, one should expect that recrystallization of the NWs can produce a reversible effect with

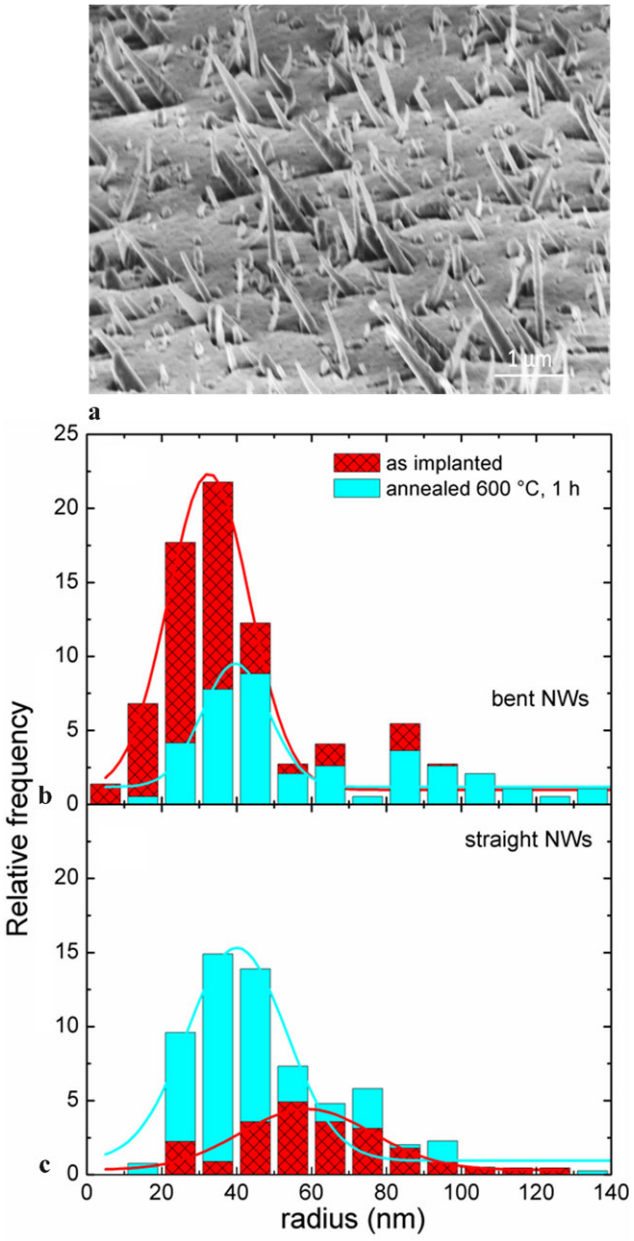

Fig. 5 (**a**) SEM image of the sample implanted and annealed at the temperatures of 600°C for 1 hour under N_2 flowing gas. Histogram plot of the measured bent (**b**) and straight (**c**) NW frequency as a function of the radius

bent NWs able to be straightened again. We have therefore investigated the damage recovery kinetics through thermal annealing at temperatures of 600°C and 800°C for 1 hour under N_2 flowing gas. A SEM image of the sample first irradiated at 1×10^{15} Ge/cm^2 and then annealed at 600°C is shown in the Fig. 5(a). The difference with the image of the same sample before the thermal treatment (Fig. 2(a)) is impressive: most of the NWs are now straight, thus indicating that a recovery of the structure has been obtained. We measured the mean length of the straight NWs in this sample and the value is in full agreement with the mean length of the NWs in the as-deposited sample. This check ensures us that the straight NWs which we are analyzing have not been broken during the annealing, but they actually have bent in consequence of the thermal process getting back to their original structure after annealing.

In order to gain more information on the process and on its size dependence, we measured the concentration of bent and straight NWs as a function of base radius in the annealed sample. Panel (b) in Fig. 5 reports the histogram plot of the bent NWs frequency as a function of the radius, while panel (c) refers to the straight NWs. The as-implanted sample is also reported as a reference together with the sample annealed at 600°C. Data are fitted through a Gaussian function (continuous line) to determine the mean size of each distribution. First of all, while ∼70% of the NW population was bent after implantation, after annealing at 600°C this population is reduced to ∼35% while ∼65% of the NWs are now straight. The size dependence is also very important. The mean size of the straight NWs is strongly reduced from ∼60 nm to ∼40 nm, implying that, after annealing, the distribution of straight NWs comprehends the smallest NWs in the sample, which were bent before the annealing in consequence of the irradiation. This value does not change anymore with increasing the annealing temperature.

Important information on the unbending process can be gained by the structural analysis of annealed NWs. Figure 6 shows the TEM analyses of the NWs after the annealing treatment at 600°C. We analyzed both the straight and the bent NWs in order to deeply understand the recrystallization kinetics. Figure 6(a) shows the bright field and the relative diffraction pattern of one of the recovered NWs. It exhibits a single-crystal structure, as confirmed by the diffraction spots, with many extended defects such as twins, visible through the extra spots in the diffraction pattern. It demonstrates that the crystalline strip we observed before the annealing in the NW acts as a seed driving a Solid Phase Epitaxial (SPE) regrowth process within the NW. This recrystallization eliminates the amorphous and produces a straightening of the NWs. Thus, the observed bending is a direct effect of the presence of the amorphous structure in the NW and it is fully reversible as soon as the amorphous region is recovered. The question arises of why some NWs then remain bent. Figure 6(b) shows the bright field TEM image and the diffraction pattern of one of the NWs, which remained bent even after the annealing procedure. In this case we observe a very different structural feature. In fact, the TEM analyses suggest that the crystalline strip did not drive the epitaxial regrowth; indeed the NW remained partially amorphous and bent. Moreover, some dark spots are visible in the bright field and the analysis of the diffraction pattern confirms that these spots are related to crystalline grains in the NW. Random Nucleation and Growth (RNG) occurred,

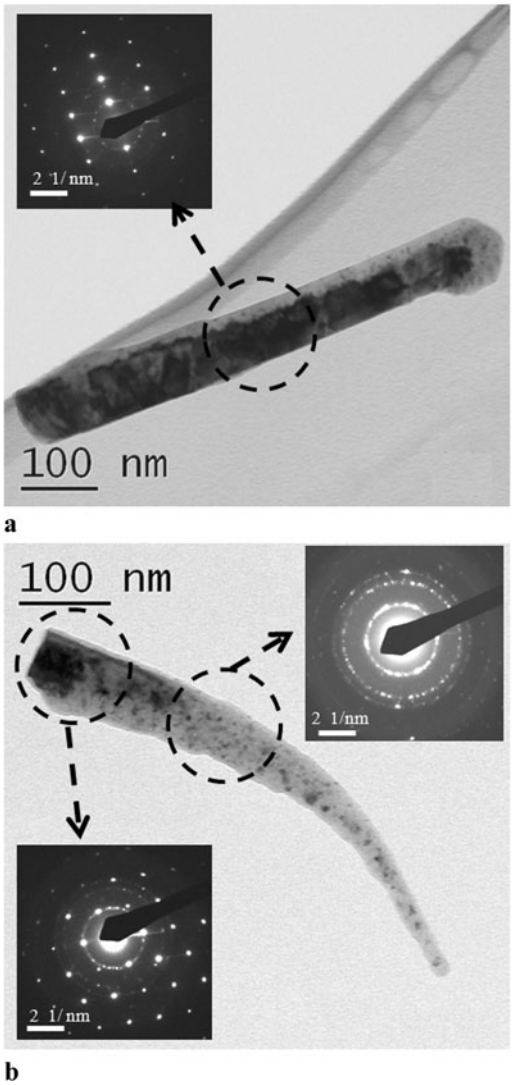

Fig. 6 Bright field image and Selected Area Diffraction patterns of (**a**) straight and (**b**) bent NWs after the annealing procedure

leading to polycrystalline grains all over the structure. It is very intriguing to note that the density of these grains as well as their mean size is larger in the base of the NW; indeed in the top of the NW, where its radius is smaller than in the base, they can be found more rarely and they are smaller. It is clear now that some NWs remained bent because no SPE occurred. This suggests that, as for the recrystallization of Si nanoclusters [25], size effects play a crucial role in the crystallization at the nanoscale. In fact in small NWs the RNG process is much less probable (as reported for nanoclusters [24]) and hence, in the competition, SPE can take place. In contrast in larger NWs, close to the single-crystal seed, RNG occurs inhibiting SPE. It should be observed that RNG process begins at a temperature of 600°C, which is lower than the temperature observed for such processes in bulk Si. It is reasonable to expect that some Au contaminations are inside the NW, and it is well known that the RNG processes in presence of metals occur at lower temperatures [26].

4 Conclusions

In conclusion, we have presented a detailed and complete study on the effects of the ion irradiation on the Si NWs structural features with the aim to address the use of ion implantation as the standard doping technique for Si NWs. Whenever Si NWs are amorphized, the NW structure will be affected, so limiting the highest dopant concentration achievable in these nanostructures. In particular the NWs bend toward the beam in such a way to minimize the exposed area to the beam and to accommodate the internal stresses caused by the formation of a crystal/amorphous interface. This process is reversible and annealing treatments can determine a phase change in the NW structure with a recrystallization and a simultaneous unbending. This process, however, is size dependent, occurring mainly in the smallest NWs. These results have strong implications on the possibility to efficiently dope Si NWs through ion implantation.

Acknowledgements We thank Carmelo Percolla, Salvo Tatì and Corrado Bongiorno for expert technical assistance.

References

1. S.W. Chung, J.Y. Yu, J.R. Heath, Appl. Phys. Lett. **76**, 2068 (2000)
2. Y. Cui, Z. Zhong, D. Wang, W.U. Wang, C.M. Lieber, Nano Lett. **3**, 149 (2003)
3. B. Tian, X. Zheng, T.J. Kempa, Y. Fang, N. Yu, G. Yu, J. Huang, C.M. Lieber, Nature **449**, 885 (2007)
4. B. Tian, T.J. Kempa, C.M. Lieber, Chem. Soc. Rev. **38**, 16 (2009)
5. Y. Cui, Q. Wei, H. Park, C.M. Lieber, Science **293**, 5533 (2001)
6. C.K. Chan, H. Peng, G. Liu, K. McIlwrath, X.F. Zhang, R.A. Huggins, Y. Cui, Nat. Nanotechnol. **3**, 31 (2008)
7. E. Tutuc, J. Appenzeller, M.C. Reuter, S. Guha, Nano Lett. **6**, 2070 (2006)
8. P.D. Kanungo, N. Zakharov, J. Bauer, O. Breitenstein, P. Werner, U. Goesele, Appl. Phys. Lett. **92**, 263107 (2008)
9. M. Schmid, M.T. Bjork, J. Knoch, S. Karg, H. Riel, W. Riess, Nano Lett. **9**, 173 (2009)
10. A. Colli, A. Fasoli, C. Ronning, S. Pisana, S. Piscanec, A.C. Ferrari, Nano Lett. **8**, 2188 (2008)
11. S. Hoffmann, J. Bauer, C. Ronning, T. Stelzner, J. Michler, C. Ballif, V. Sivakov, S.H. Christiansen, Nano Lett. **9**, 1341 (2009)
12. P.D. Kanungo, R. Kogler, K. Nguyen-Duc, N. Zakharov, P. Werner, U. Gosele, Nanotechnology **20**, 165706 (2009)
13. C. Borschel, R. Niepelt, S. Geburt, C. Gutsche, I. Regolin, W. Prost, F.J. Tegude, D. Stichtenoth, D. Schwen, C. Ronning, Small **5**, 2576 (2009)
14. L. Romano, N.G. Rudawski, M.R. Holzworth, K.S. Jones, S.G. Choi, S.T. Picraux, J. Appl. Phys. **106**, 114316 (2009)
15. K. Jun, J. Joo, J.M. Jacobson, J. Vac. Sci. Technol. B **27**, 3043 (2009)
16. B.C. Park, K.Y. Jung, W.Y. Song, B.-h. O, S.J. Ahn, Adv. Mater. **18**, 95 (2005)

17. D. Stichtenoth, K. Wegener, C. Gutsche, I. Regolin, F.J. Tegude, W. Prost, M. Seibt, C. Ronning, Appl. Phys. Lett. **92**, 163107 (2008)
18. A. Irrera, E.F. Pecora, F. Priolo, Nanotechnology **20**, 135601 (2009)
19. E.F. Pecora, A. Irrera, F. Priolo, Thin Solid Film **518**, 2562 (2010)
20. E. Rimini, *Ion Implantation: Basics to Device Fabrication* (Kluwer Academic, Dordrecht, 1995)
21. C.A. Volkert, J. Appl. Phys. **70**, 3521 (1991)
22. T. van Dillen, A. Polman, C.M. van Kats, A. van Blaaderen, Appl. Phys. Lett. **83**, 4315 (2003)
23. T. van Dillen, M.J.A. de Dood, J.J. Penninkhof, A. Polman, S. Roorda, A.M. Vredenberg, Appl. Phys. Lett. **84**, 3591 (2004)
24. H. Trinkaus, A.I. Ryazanov, Phys. Rev. Lett. **74**, 5072 (1995)
25. F. Iacona, C. Bongiorno, C. Spinella, S. Boninelli, F. Priolo, J. Appl. Phys. **95**, 3723 (2004)
26. C. Spinella, S. Lombardo, F. Priolo, J. Appl. Phys. **84**, 5383 (1998)